Available online at www.sciencedirect.com
SCIENCE DIRECT®
Microelectronic Engineering 69 (2003) 261–264
MICROELECTRONIC ENGINEERING
www.elsevier.com/locate/mee

The influence of many body and electron nonparabolicity effects in the intersubband optical spectra of III–V quantum wells

M.F. Pereira Jr[a,*,1], H. Wenzel[b]

[a]NMRC, University College, Lee Maltings, Prospect Row, Cork, Ireland
[b]Ferdinand-Braun-Institut fuer Hoechstfrequenztechnik, Berlin Rudower Chaussee 5, D-12489 Berlin, Germany

Abstract

In this paper, effective masses adjusted to the non parabolic electron subbands obtained from the solutions of an 8×8 KP Hamiltonian are used as input for a many particle optical susceptibility solver capable of consistently taking into account exchange and depolarisation effects through numerical inversion of the Keldysh Green's functions equations for the optical polarisation. Numerical results are presented for III–V quantum wells.

Keywords: Electron nonparabolicity; Many body effects; Intersubband transitions

1. Introduction

Novel optoelectronic devices whose operation is based upon intersubband transitions open new possibilities in the infrared region [1–3]. Notably, the absorption, gain and refractive index spectra can be tailored to specific applications with a high flexibility dependent almost solely on the design of the structure and not on the actual material parameters. In this paper, to the best of the authors knowledge, the non parabolic electron subbands obtained from the solutions of an 8×8 KP Hamiltonian [4,5] are used as input for a many particle optical susceptibility solver capable of consistently taking into account exchange and depolarization effects through numerical inversion of the nonequilibrium Keldysh Green's functions equations for the optical polarisation. Numerical results are presented for III–V quantum wells for different design, temperature and excitation conditions, and the interplay between many particle and non parabolic band structure effects is discussed. Scattering beyond the exchange approximation and its influence in the line shape of the transitions is further discussed within a scheme that allows the calculation of increasingly higher order Coulomb correlations under equilibrium and nonequilibrium conditions.

2. Main equations

Charged carriers in semiconductors can be investigated at a microscopic level by means of a nonequilibrium Keldysh Green's function, $i\hbar G(\underline{12}) = \langle \Psi(\underline{1})\Psi\dagger(\underline{2})\rangle$, where $\Psi(\underline{1})$ is the electron field operator. The quantum mechanical averages are calculated along the double-time Keldysh contour, C [6]. The Keldysh Green's function time evolution is

*Corresponding author. Present address: TU Berlin Institut fur Theoretische Physik, Berlin 10623, Germany. Tel.: +49-30-314-24858; fax: +49-30-314-21130.
E-mail address: mpereira@nmrc.ucc.ie (M.F. Pereira Jr).
[1]Research supported by SFI, Ireland.

0167-9317/03/$ – see front matter
doi:10.1016/S0167-9317(03)00306-X

described by a Dyson equation (sum over repeated arguments is assumed):

$$[G_o^{-1}(\underline{13}) - \Sigma(\underline{13})]G(\underline{32}) = \delta(\underline{12}). \quad (1)$$

The carriers self energy includes scattering and leads to bandgap renormalisation and spectral broadening. Electron–electron scattering is described by:

$$\Sigma(\underline{12}) = -i\hbar e G(\underline{13})W(\underline{41})\gamma(\underline{324}), \quad (2)$$

where we have introduced the vertex function,

$$\gamma(\underline{123}) = -e\delta(\underline{13})\delta(\underline{12}) + \frac{\delta\Sigma(\underline{12})}{\delta G(\underline{45})} G(\underline{46})\gamma(\underline{673})G(\underline{75}), \quad (3)$$

by means of which, increasingly higher order Coulomb corrections can be evaluated.

3. Approximate solution for the dynamical equations

The optical and transport properties of a given structure are derived from solutions of the Dyson equations for the proper projected quantities. Projecting into Keldysh indices and separating explicitly the retarded, *r* and advanced *a* self energies into its exchange, *x* and correlation, *c* components, lead, e.g. to:

$$\Sigma^r(\underline{12}) = \Sigma^x(\underline{12}) + \Sigma^c(\underline{12}), \quad (4)$$

which contains spectral information.

We are interested in the projection onto the $[ji]$ coupling that yields optical and tunnelling transition rates between states *i* and *j*. If the eigenstate for level *j* characterised by labels *j* and *k* for the quasimomentum corresponding to energy $\hbar\epsilon_j(k)$ is denoted $\phi_{jk}(R)$, $R \equiv (\vec{r}, z)$, the field operators used in our Green's functions are then expanded as:

$$\Psi(\vec{R}) = \sum_{j,\vec{k}} \frac{1}{\sqrt{S}} e^{i\vec{k}\vec{r}} \phi_j(z) a_{j,\vec{k}}, \quad (5)$$

and the relevant equation of motion in the physical limit, $t_1 = t_2 = t$, reads:

$$\begin{aligned} &i\hbar\left(\frac{\partial}{\partial t} + e_j(k) - e_i(k)\right)G_{ji}^<(k,t) \\ &+ \vec{\mathscr{P}}_{ji}(k)\vec{E}(t)(G_{ii}^<(k,t) - G_{jj}^<(k,t)) \\ &+ i\hbar(G_{jj}^<(k,t) - G_{ii}^<(k,t))2V\begin{pmatrix} j & i & i & j \\ 0 & & & \end{pmatrix} \\ &\times \sum_{\vec{k}'} G_{ji}^<(k',t) - i\hbar(G_{jj}^<(k,t) - G_{ii}^<(k,t)) \\ &\times \sum_{\vec{k}'} G_{ji}^<(k',t)V\begin{pmatrix} j & j & i & i \\ k & k' & k & k' \end{pmatrix} = I_{ji}(k,t). \end{aligned} \quad (6)$$

The left hand side has the Hartree–Fock contribution while the RHS has correlation terms, which include, e.g. electron–electron scattering and non-diagonal dephasing. The correlation contribution will be described in detail in the next report. Here, we replace it by a constant dephasing term. The bare Coulomb interaction and renormalised energies, which appear above, are given by:

$$\begin{aligned} V\begin{pmatrix} n & m & l & p \\ k_n & k_m & k_l & k_p \end{pmatrix} &= \delta_{\vec{k}_n - \vec{k}_m, \vec{k}_l - \vec{k}_p} V^{2d}_{\vec{k}_n - \vec{k}_m} \\ &\times \int \phi_n^*(z)\phi_m(z)V(R - \\ R')\phi_l^*(z)\phi_p(z')e^{-|\vec{k}_n - \vec{k}_m||z - z'|}\,dz\,dz' \end{aligned} \quad (7)$$

$$\begin{aligned} \hbar e_j(k) = \hbar\epsilon_j(k) &+ \sum_{\vec{k}'} G_{jj}^<(k',t)i\hbar V\begin{pmatrix} j & j & j & j \\ k & k' & k & k' \end{pmatrix} \\ &+ \sum_{\vec{k}'} G_{jj}^<(k',t)i\hbar V\begin{pmatrix} j & i & i & i \\ k & k' & k & k' \end{pmatrix}. \end{aligned}$$

4. Numerical results and discussion

In what follows we show absorption spectra assuming the carriers thermalised in quasi-equilibrium in the various subbands. A full description of gain in the nonequilibrium regime including electron–electron interactions currently under investigation. The equilibrium results given here already go beyond previous theories [7] found in the literature which use a simplifying ansatz in which full Coulomb coupling terms are replaced by averages. In contrast to these theories, we solve our equations exactly, without making use of this ansatz, by means of a numerical matrix inversion technique that extends previous methods successfully used for

conventional semiconductor lasers [8]. Furthermore, instead of phenomenological dephasing parameters, we use calculated electron–electron scattering matrix elements. The interplay between different many-particle corrections, e.g. exchange and depolarization contributions, are included in the numerics. The general theory supports higher order Coulomb scattering beyond the screened Hartree–Fock level, but these processes, as well as phonon and impurity scattering which broaden the spectral lines, are neglected here, where we want to illustrate the principal phenomena.

The dotted lines of Fig. 1 illustrate the nonparabolic conduction subbands of a 9 nm InGaAsP/GaAsP quantum well. computed with an 8×8 KP Hamiltonian [4].

As a first step in the evaluation of nonparabolicity effects, we fit each conduction subband with a parabolic band. From top to bottom, the resulting effective masses are: $m_{\rm eff}=0.086$, 0.099, 0.112, 0.111, $0.115\times m_0$, where m_0 is the free electron mass. We use those adjusted masses in the computations that follow. The dot-dashed are the corresponding dispersion relations.

Different transitions contribute to the total spectra. In the discussion that follows, we denote by (i, j) a transition between a lower level 'i' and upper level 'j'.

The interplay between different effective masses and many particle effects on the intersubband optical absorption can be illustrated in Fig. 2. A density of

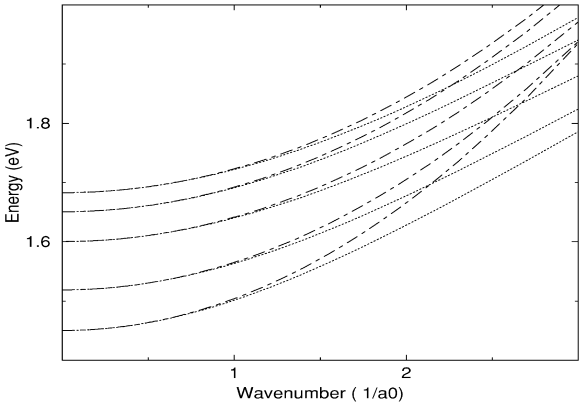

Fig. 1. Nonparabolic (dots) and effective parabolic conduction subbands (dot-dashed) of a 9 nm InGaAsP/GaAsP quantum well.

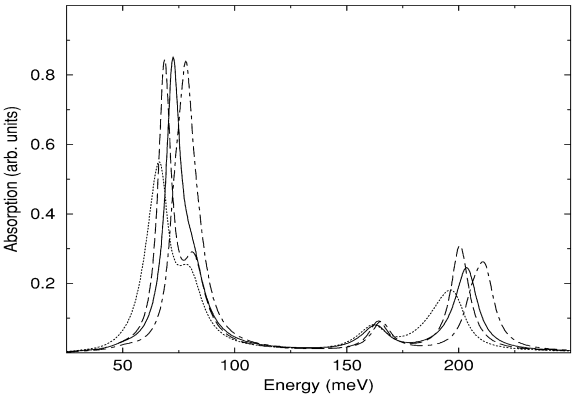

Fig. 2. Intersubband absorption spectra at $T=300$ K and $N=10^{11}$ carriers per cm^2 for the same structure of Fig. 1. The solid and dot-dashed curves have many particle corrections, while the dotted and long-dashed curves are for free carriers. Effective nonparabolicty as discussed in the text is included in the solid and dotted curves, while the dot-dashed and long-dashed have the same effective mass in all subbands.

$N=10^{11}$ carriers per cm^2 is distributed in equilibrium among the five conduction subbands at 300 K. Carrier–carrier dephasing is accounted for by evaluating the statically screened lowest order GW self energy at $k=0$ at the subband gap. The solid and dot-dashed curves have many particle corrections, while the dotted and long-dashed curves are for free carriers. Effective nonparabolicty as discussed in the text is included in the solid and dotted curves, while the dot-dashed and long-dashed have the same effective mass in all subbands i.e. $m_{\rm eff}=0.086$.

Note that in the dispersive case (different masses), the Coulomb corrections increase considerably the peak absorption value and reduces the bandwidth. The effect is of course stronger on the main structure around 75 meV in the low energy side and on the structure around 200 meV. The reason is the higher occupation of the first band leading to higher population differences. Note that the main contributions at the low energy side are from transitions (1, 2) and (2, 3), while on the high energy side from (1, 4), and (2, 5) makes the contribution around 162 meV. It is clear from the figure that, even at lowest order, both nonparabolicity and many body effects must be taken into account for consistent calculations.

In summary, the numerical results given in this paper show that, even at lowest order, conduction

band nonparabolicity and many particle effects can be very important and a consistent theory for the optical properties of intersubband devices may have to consider all these effects together. It is clear that nonparabolicity was not included here fully in the dispersion relations and most importantly also not in the transition dipole moments, which indicates that the combined effects may be even larger. Their relevance is current under investigation. Furthermore, higher order Coulomb corrections, which are actually supported in the theory have not been considered here, but are also currently being implemented and shall be the subject of future publications. We hope that the numerical simulations presented here will stimulate new experimental efforts to clarify the importance of many body and electron nonparabolicity in the Physics and development of new intersubband transition based devices.

References

[1] J. Faist et al., Phys. Rev. Lett. 71 (1993) 3573.
[2] C. Sirtori et al., Appl. Phys. Lett. 73 (1998) 3486.
[3] S.-C. Lee, A. Wacker, Physica E13 (2002) 858–861.
[4] H. Wenzel, G. Erbert, P. Enders, IEEE J. Select. Top. Quantum Electron. 5 (1999) 637.
[5] M.F. Pereira Jr, H. Wenzel, Phys. Stat. Sol. (b) 232 (2002) 134.
[6] L.V. Keldysh, Zh. Eksp. Teor. Fiz. Sov. Phys. JETP 20 (1965) 4.
[7] D.E. Nikonov et al., Phys. Rev. Lett. 79 (1997) 4633.
[8] M.F. Pereira Jr, K. Henneberger, Phys. Rev. B58 (1998) 2064.